CrystEngComm

PAPER

View Article Online
View Journal | View Issue

Cite this: *CrystEngComm*, 2014, **16**, 3540

Morphology tuning in the formation of vaterite crystal thin films with thermoresponsive poly(*N*-isopropylacrylamide) brush matrices†

Yulai Han, Tatsuya Nishimura* and Takashi Kato*

Received 29th December 2013,
Accepted 26th February 2014

DOI: 10.1039/c3ce42646g

www.rsc.org/crystengcomm

The use of a thermoresponsive polymer brush matrix resulted in the formation and morphology tuning of $CaCO_3$ crystal thin films. Poly(*N*-isopropylacrylamide) (PNIPAm) brushes with thickness of approximately 500 nm were synthesized and employed as crystallization templates for $CaCO_3$. The PNIPAm brush matrix induced the formation of vaterite thin films in the presence of poly(acrylic acid). Moreover, crystallization of $CaCO_3$ at temperatures above and below the lower critical solution temperature of the PNIPAm brush matrices led to the preparation of vaterite films with distinctly different crystallographic orientations. The approach of using a stimuli-responsive polymer brush matrix may provide a novel way for the development of hybrid coating materials.

Introduction

Biominerals such as the nacre of shells, bones and teeth are organic/inorganic composites synthesized naturally by living organisms.[1–3] These biominerals exhibit elaborate structures that function as structural supports, protection and mineral storage. The biomineralization process has been inspiring materials scientists for the last two decades to develop functional composites under mild conditions.[4–19] Cooperation of insoluble macromolecular templates and soluble acidic biomacromolecules is crucial in biomineralization.[20–22] For synthetic materials, $CaCO_3$ crystal thin films have also been successfully synthesized *via* the bio-inspired approach.[4,7,23–25]

A variety of polymer templates have been used as templates for biomimetic synthesis of inorganic crystals.[26,27] Our previous studies have shown that insoluble polymer matrices, such as poly(vinyl alcohol) (PVA), chitin and chitosan, promoted the formation of thin films of calcium carbonate crystals.[7,28,29]

Among the coating methods of polymer templates which are subsequently used as crystallization matrices for inorganic crystals,[7] polymer brushes are attractive as new templates because of the density of their functional groups on the surface. Polymer brushes are thin polymer coatings consisting of polymer chains with the termini covalently fixed to a substrate, and such polymer layers possess excellent long-time stability in various solvents at a wide range of temperatures.[30–32] Recent advancements on surface-initiated controlled radical polymerization techniques, such as atom transfer radical polymerization (ATRP), enabled the precise control of the thickness, composition and architecture of the polymer brushes.[33–35] Surface-initiated ATRP allows the modification of various surfaces, such as silicon, metal oxides[36] and polymer surfaces,[37] by covalently attached polymer brushes. Thus, a study of the crystallization behavior of inorganic minerals on polymer brush matrices may provide useful information toward the design of organic/inorganic functional hybrid coating materials. However, only very limited examples of inorganic crystallization on polymer brush matrices have been reported.[23,38]

In biomineralization, morphological and orientational selection is of significant importance to living organisms since it is closely related to the functional properties of the resultant biominerals.[1–3,39,40] Recently, stimuli-responsive polymers have attracted a great deal of attention.[41–43] In artificial biomimetic systems, the use of stimuli-responsive polymer matrices is a promising method for the realization of the morphological and orientational control of mineral crystals. We have previously reported the use of a photoresponsive polymer matrix for the successful control of the morphologies of $CaCO_3$ crystal thin films.[25] On the other hand, PNIPAm is a thermoresponsive polymer that exhibits lower critical solution temperature (LCST) in water at around 32 °C.[44] PNIPAm brushes exhibit an aggregated conformational structure due to the intramolecular hydrogen bonding between C═O and N–H at temperatures above its LCST, while at temperatures below the LCST, a stretched conformational structure is adopted because of hydrogen bonding interactions with water molecules.[45,46] PNIPAm coatings have been widely used as bioactive matrices for cell cultivation, showing reversible cell attachment and

Department of Chemistry and Biotechnology, School of Engineering, The University of Tokyo, Bunkyo-ku, Tokyo 113-8656, Japan.
E-mail: tatsuya@chembio.t.u-tokyo.ac.jp, kato@chiral.t.u-tokyo.ac.jp

† Electronic supplementary information (ESI) available. See DOI: 10.1039/c3ce42646g

detachment properties at temperatures above and below the LCST.[47–49] When PNIPAm brushes were used as crystallization matrices, our previous study showed that the use of PNIPAm brush matrices induced the formation of unidirectionally oriented fibrous calcium carbonate at a temperature above the LCST.[23] Generally, many polymer template surfaces could promote the formation of inorganic nuclei by decreasing the activation energy of nucleation,[50,51] and the conformational change of polymer chains in the template is likely to influence the crystallization behavior of minerals. Thus, the conformational rearrangements of the PNIPAm brush chains across the LCST are expected to induce the formation of crystals with different morphologies (Fig. 1). Herein, we report on the study of the crystallization of $CaCO_3$ on thermoresponsive PNIPAm brush matrices at temperatures above and below the LCST.

Experimental

Materials

N,*N*,*N*′,*N*″,*N*″-pentamethyldiethylenetriamine (PMDETA) and poly(acrylic acid) (PAA, M_w = 2.0 × 10^3) were purchased from Aldrich. Triethylamine (99%), (3-aminopropyl)triethoxysilane (99%), 2-bromo-2-methylpropionyl bromide (98%), and *N*-isopropylacrylamide (NIPAm, 97%) were purchased from Tokyo Kasei. Copper(I) bromide (CuBr, 99.7%), methanol (MeOH, 99.5%), calcium chloride, ammonium carbonate and ethanol (anhydrous, 99.5%) were obtained from Wako. NIPAm was purified by vacuum sublimation. PMDETA was vacuum-distilled prior to use. All other chemicals were used as received without further purification.

Preparation of ATRP-initiator deposited silicon and glass substrates

The synthesis of PNIPAm brushes followed the procedures given in Scheme 1. Firstly, 2-bromo-2-methyl-*N*-(3-triethoxysilyl-propyl)-propionamide (ATRP-initiator) was synthesized by the condensation of (3-aminopropyl)trimethoxysilane and 2-bromo-2-methylpropionyl bromide. The silicon and glass substrates were placed in an oxygen plasma treatment chamber (Cute-1MP, Femto Science) filled with pure oxygen to clean the surface for 5 min (100 W). Subsequently, the slides were immersed in 30 mM solution of the ATRP-initiator in anhydrous ethanol for 24 h at 25 °C. The resultant slides were washed with ethanol, sonicated in ethanol for 1 min, and dried with a stream of nitrogen.

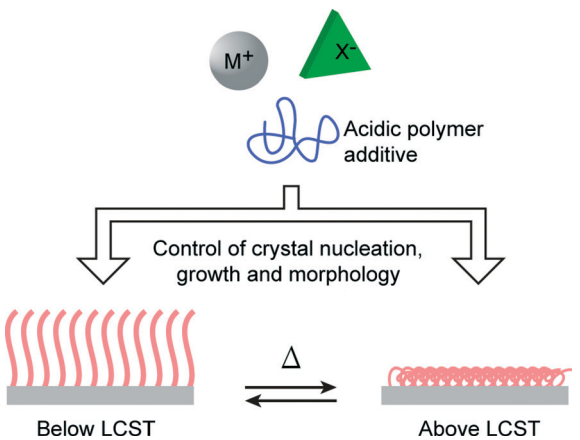

Fig. 1 Schematic illustration of the approach of using thermoresponsive PNIPAm brush matrices for controlling crystal nucleation, growth and morphology.

Synthesis of PNIPAm brushes from ATRP-initiator modified substrates

In a typical ratio of [NIPAm]:[CuBr]:[PMDETA] = 200:1:5, 2 g of NIPAm, 6 ml of deionized water and 2 ml of methanol were added into a Schlenk flask, and the solution was degassed by three freeze–pump–thaw cycles. CuBr (12 mg) and PMDETA (60 mg) were added into the deoxygenated solution. Subsequently, the solution was transferred into a nitrogen purged reaction vessel containing the ATRP-initiator modified substrates. The reaction was allowed to proceed for 1 h. After polymerization, substrates grafted with PNIPAm brushes were taken from the polymerization solution, rinsed with large quantities of methanol and deionized water, and dried with a stream of nitrogen.

Crystallization of calcium carbonate on substrates grafted with PNIPAm brushes

Purified water obtained from an Auto pure WT100 purification system (Yamato, relative resistivity: maximum 1.8 × 10^7 Ω cm) was employed for $CaCO_3$ crystallization. Calcium chloride aqueous solution ([Ca^{2+}] = 10 mM) containing PAA (2.5 × 10^{-3} wt%) was used to carry out $CaCO_3$ crystallization. The solution was transferred into vessels containing the matrices grafted with PNIPAm brushes. The vessels were then placed in a closed desiccator together with ammonium carbonate. An incubator (Fukushima) was used to maintain a constant crystallization temperature. $CaCO_3$ crystallization at 20 °C (below the LSCT) and 40 °C (above the LSCT) was carried out in this study.

Characterization

Fourier transform infrared (FTIR) spectra were recorded using a Jasco FT/IR-6100 spectrometer (Jasco, Tokyo). The brush thickness was determined using a Jasco M-500 ellipsometer (Jasco, Tokyo) equipped with a He–Ne laser (λ = 632.8 nm). The thickness was further examined by tapping-mode atomic force microscopy (AFM) measurements (Bruker, Santa Barbara). Scanning electron microscopy (SEM) images were obtained using a Hitachi S-4700 field-emission SEM (Hitachi, Tokyo) operated at 3–5 kV. Samples were coated with a layer of platinum using a Hitachi E-1030 ion sputter (Hitachi, Tokyo). Polarizing optical microscope images were taken using an Olympus BX51 polarizing optical microscope (Olympus, Tokyo). Raman spectra were obtained using a Jasco Model NR-1800 spectrometer (Jasco, Tokyo) with an excitation source of Nd:YAG laser (532 nm). X-ray diffraction (XRD) measurements were performed using a Rigaku SmartLab Intelligent X-ray Diffraction System (Rigaku, Tokyo) with filtered Cu Kα radiation (λ = 1.5406 Å, operating at 40 kV and 40 mA). Transmission electron

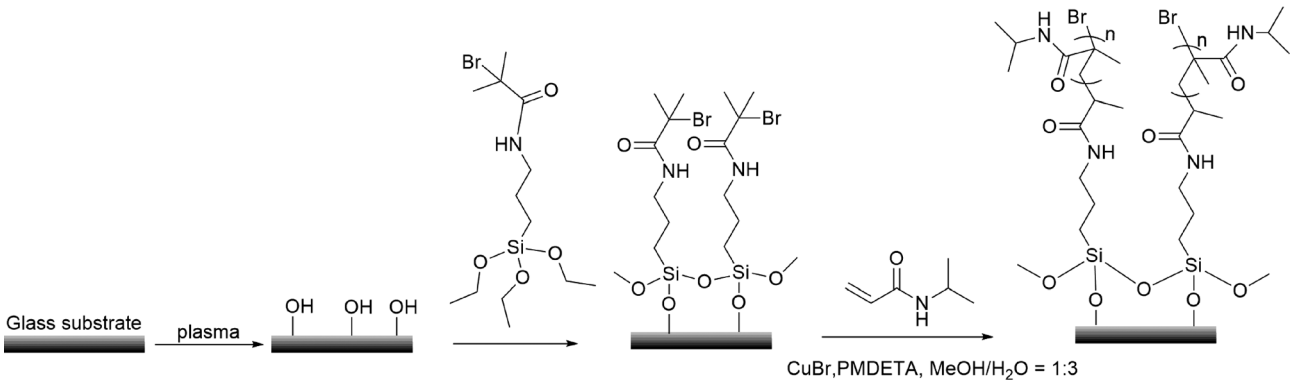

Scheme 1 Procedures for the synthesis of PNIPAm brushes *via* surface-initiated ATRP.

microscopy (TEM) images were taken using a JEOL JEM-2010HC operated at 200 kV.

Results and discussion

Characterization of PNIPAm brush matrices synthesized *via* surface-initiated ATRP

The surface morphology of the PNIPAm brush substrates synthesized *via* surface-initiated ATRP was measured by AFM. Fig. 2a shows the three-dimensional AFM image of the PNIPAm grafted substrate surface. The synthesized PNIPAm brushes have a root-mean-square roughness (R_{RMS}) value of about 0.5 nm over a 1 μm × 1 μm area. No aggregation of the chains was observed, which shows that the brush surface is uniform and homogeneous. The formation of PNIPAm brushes was also confirmed by IR spectroscopy (Fig. 2b). The absorption peak at 3302 cm^{-1} corresponds to the stretching of the amide N–H group. The anti-symmetric stretching vibration of the CH_3 group gives rise to the peak at 2970 cm^{-1}. The strong absorption peak at 1649 cm^{-1} can be attributed to the secondary amide C═O stretch. The two peaks at 1386 cm^{-1} and 1365 cm^{-1} correspond to the vibration of the two methyl groups in $-C(CH_3)_2$.[52] Brush thickness was determined by AFM measurements performed across the scratched and unscratched boundaries of the brush substrate (Fig. 2c), and the corresponding depth graph shows that the brush has a thickness of approximately 500 nm in air (Fig. 2d).

Crystallization of $CaCO_3$ on PNIPAm brush matrices below the LCST

Thin films of calcium carbonate with crystal domains approximately 200 μm in diameter were formed on PNIPAm

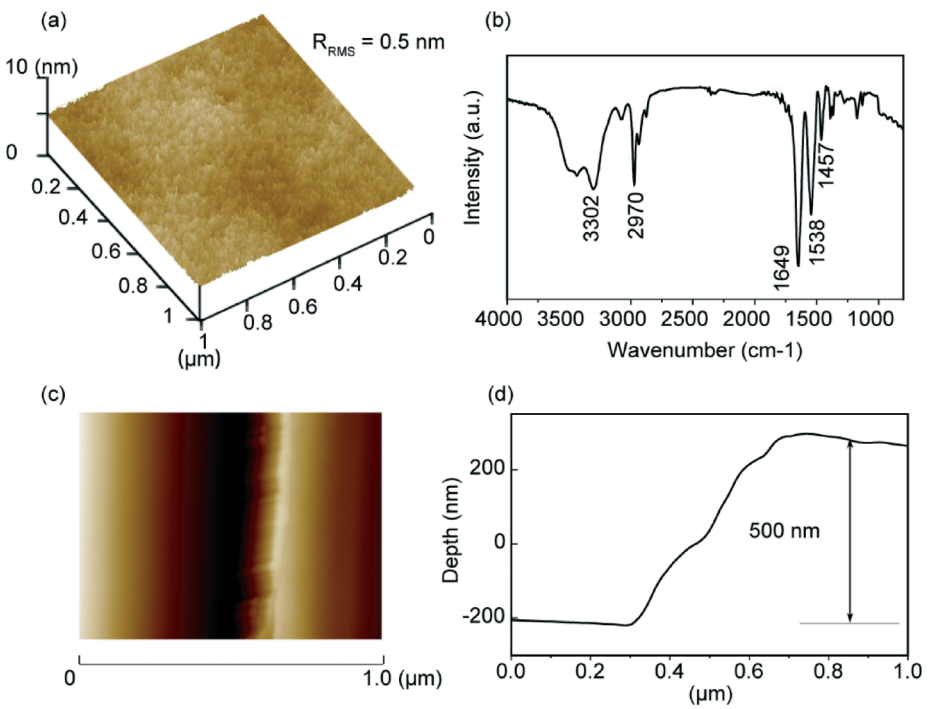

Fig. 2 Characterization of PNIPAm-grafted substrates: (a) three-dimensional AFM image of the PNIPAm-grafted silica surface, (b) IR spectrum of the PNIPAm brush, (c) AFM image across the scratched and unscratched boundaries, and (d) corresponding depth figure across the boundaries.

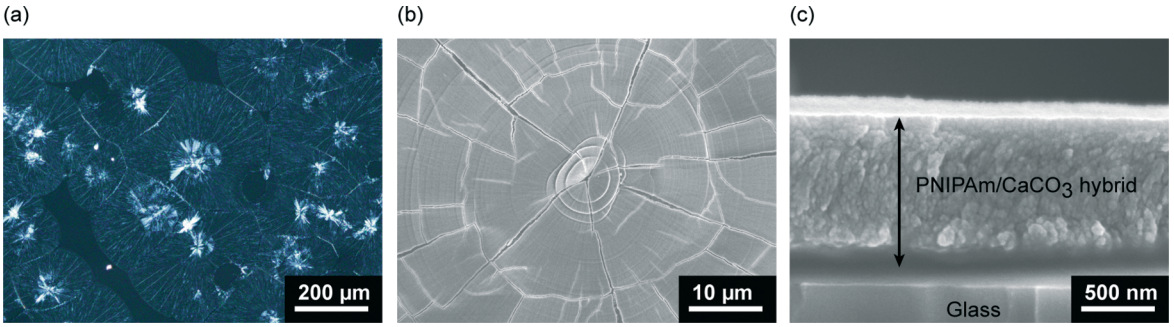

Fig. 3 $CaCO_3$ crystals developed on PNIPAm brush matrices in the presence of PAA (2.5×10^{-3} wt%) after crystallization for 10 h at 20 °C: (a) polarizing optical microscope image, (b) SEM image (top view), and (c) cross-sectional SEM image of the thin film.

brush matrices in the presence of PAA (2.5×10^{-3} wt%) when crystallization was carried out at 20 °C (Fig. 3a). The $CaCO_3$ thin films have a flat surface, although cracks along the crystal growth directions of the thin films were observed under SEM observation (Fig. 3b). The cross-sectional SEM image (Fig. 3c) reveals that the resultant thin films with thickness of about 1 μm is composed of particles approximately 50 nm in size. The Raman spectrum (Fig. 4) shows that the thin films formed at 20 °C are mainly vaterite because the corresponding Raman bands of CO_3^{2-} are observed at 1090 cm^{-1} (ν_1, symmetric stretching mode), 1075 cm^{-1} (ν_1), and 301 cm^{-1} (lattice mode).[53]

In-plane and out-of-plane XRD measurements were conducted to study the polymorph and the preferential orientation of the $CaCO_3$ crystal thin films formed at 20 °C (Fig. 5). The diffraction patterns in the XRD spectra show that the samples are mainly vaterite in morphology, which is consistent with the results obtained by Raman spectroscopy. For the thin films formed at 20 °C, diffraction peaks of the (110) and (300) planes, which are parallel to the *c* axis of the crystals, are only observed in the in-plane XRD pattern (Fig. 5a). In contrast, compared to the standard powder diffraction pattern (pdf no. 33-0268, Fig. 5c), the intensified peak assignable to the (004) plane, which is perpendicular to the *c* axis, is observed in the out-of-plane XRD pattern (Fig. 5b). These results suggest that the *c* axis in the crystal thin films formed at 20 °C is preferentially perpendicular to the substrate. The perpendicular orientation of the *c* axis was also confirmed by selected area electron diffraction (SAED) (Fig. 6), and such a preferential orientation led to dark patterns with very weak birefringence under polarizing optical microscope observation (Fig. 3a).[54] The bright-field TEM image (Fig. 6a) and the corresponding SAED pattern (Fig. 6b) also indicate that the thin films favoured the [1 $\bar{1}$ 0] growth direction.

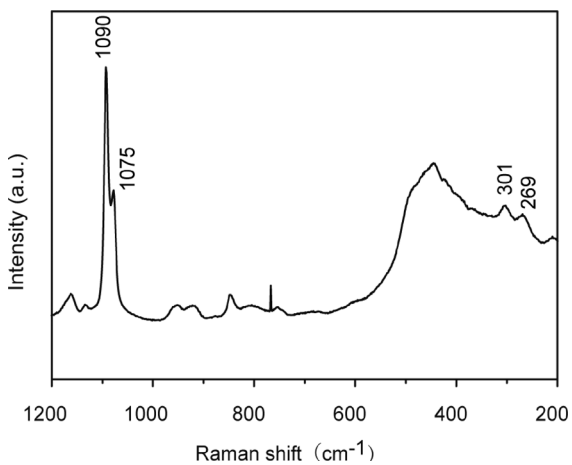

Fig. 4 Raman spectrum of $CaCO_3$ crystal thin films developed on PNIPAm brush matrices in the presence of PAA (2.5×10^{-3} wt%) after crystallization for 10 h at 20 °C.

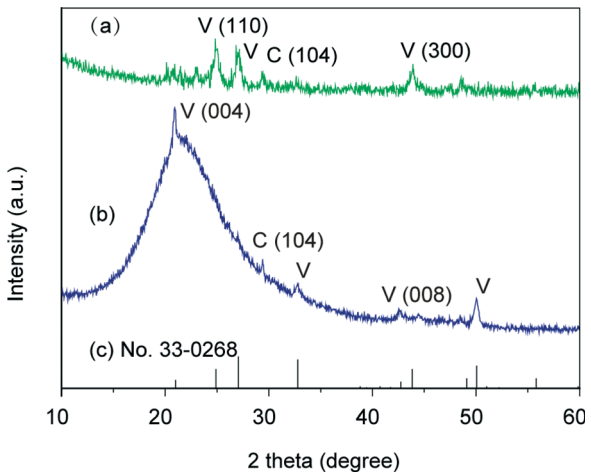

Fig. 5 XRD patterns of the $CaCO_3$ crystal thin films formed on PNIPAm brush matrices at 20 °C: (a) in-plane XRD pattern, (b) out-of-plane XRD pattern, and (c) vaterite standard powder XRD pattern from JCPDS (no. 33-0268). V and C stand for vaterite and calcite, respectively.

Crystallization of $CaCO_3$ on PNIPAm brush matrices above the LCST

Crystallization of calcium carbonate at 40 °C was also carried out to study the effect of the entangled state of the brushes on the crystallization behavior. Fig. 7a shows the polarizing optical microscope image of $CaCO_3$ crystal thin films after 6 h of crystallization at 40 °C, which is a temperature above the LSCT of PNIPAm brush matrices. Concentric spherulitic crystal thin films that exhibit mosaic patterns due to the regular orientation of the *c* axis were observed. The crystal domains

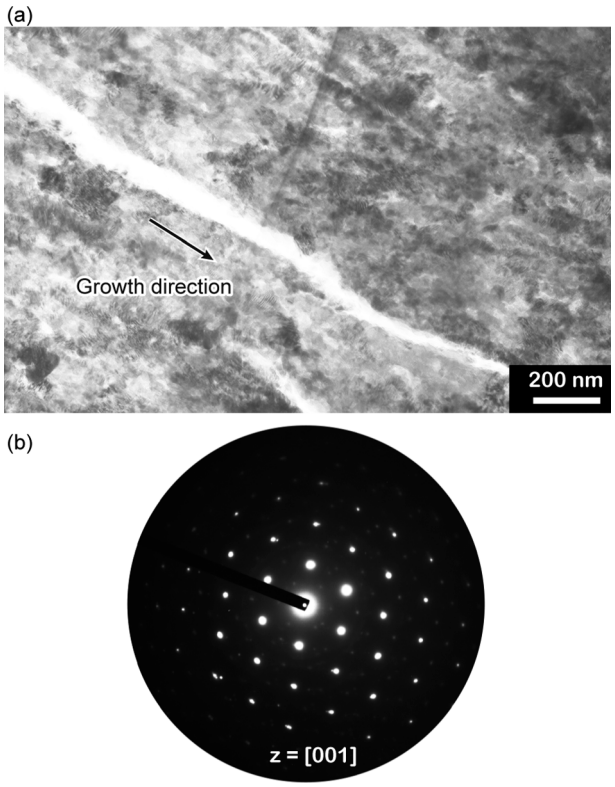

Fig. 6 (a) Bright-field TEM image and (b) corresponding SAED pattern of an isolated vaterite film grown on PNIPAm brush matrices in the presence of PAA at 20 °C. The SAED pattern shows that the thin films have a zone axis of [001].

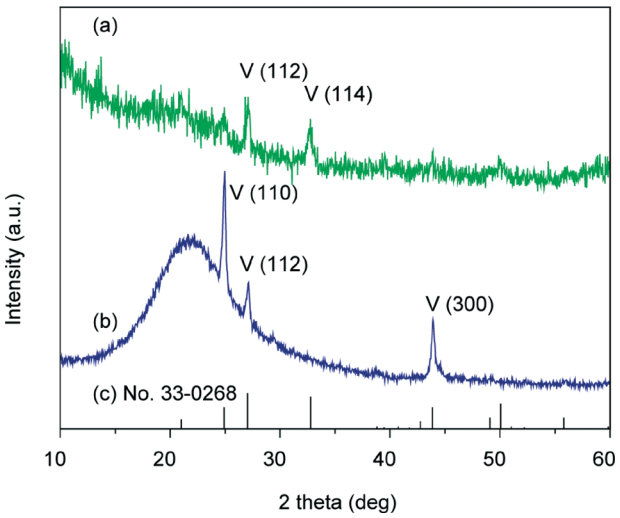

Fig. 8 XRD patterns of the $CaCO_3$ crystal thin films formed on PNIPAm brush matrices at 40 °C: (a) in-plane XRD pattern, (b) out-of-plane XRD pattern, and (c) vaterite standard powder XRD pattern from JCPDS (no. 33-0268); V stands for vaterite.

are about several hundreds of micrometers in diameter. Fig. 7b shows the SEM image of a homogeneous film surface. The thin films with thickness of about 1.5 μm are composed of polycrystalline particles approximately several tens of nanometers in size (Fig. 7c).

Both the Raman spectrum (Fig. S1 in the ESI†) and the XRD patterns of the thin films formed at 40 °C show that the crystals are of vaterite polymorph (Fig. 8). In comparison with the standard powder diffraction pattern (pdf no. 33-0268, Fig. 8c), intensified peaks of the (110) and (300) planes, which are parallel to the *c* axis, are observed in the out-of-plane XRD pattern (Fig. 8b), while the intensities of these two peaks are evidently weak in the in-plane XRD pattern (Fig. 8a). These results suggest that the $CaCO_3$ crystal thin films formed at 40 °C preferentially oriented with the *c* axis in the crystal thin films parallel to the substrate.

The orientation of the vaterite thin films formed at 40 °C was also examined by electron diffraction analysis (Fig. 9). The directions of the crystal growth and the *c* axis of the crystal thin films are shown in Fig. 9a. The SAED pattern (Fig. 9b) shows that the vaterite thin films formed at 40 °C have a zone axis of [110] and the *c* axis is aligned parallel to the surface plane of these thin films and perpendicularly oriented to the [1 $\bar{1}$ 0] growth direction.

Effects of stimuli-responsive PNIPAm brush matrices on $CaCO_3$ crystallization

It is noteworthy that vaterite, thermodynamically the least stable polymorph of anhydride $CaCO_3$,[55,56] was formed using PNIPAm brushes as crystallization matrices both above and below the LCST in the presence of PAA. For crystallization of

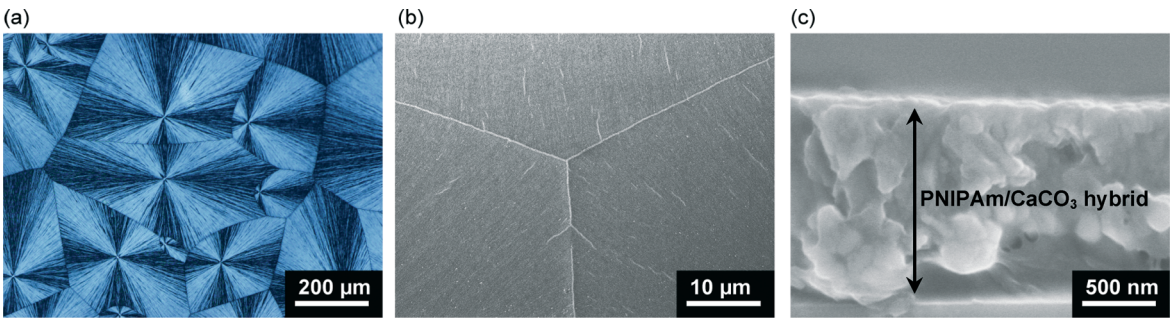

Fig. 7 $CaCO_3$ crystal thin films formed on PNIPAm brush matrices in the presence of PAA (2.5×10^{-3} wt%) after crystallization at 40 °C for 6 h: (a) polarizing optical microscope image, (b) SEM image (top view) and (c) cross-sectional SEM image.

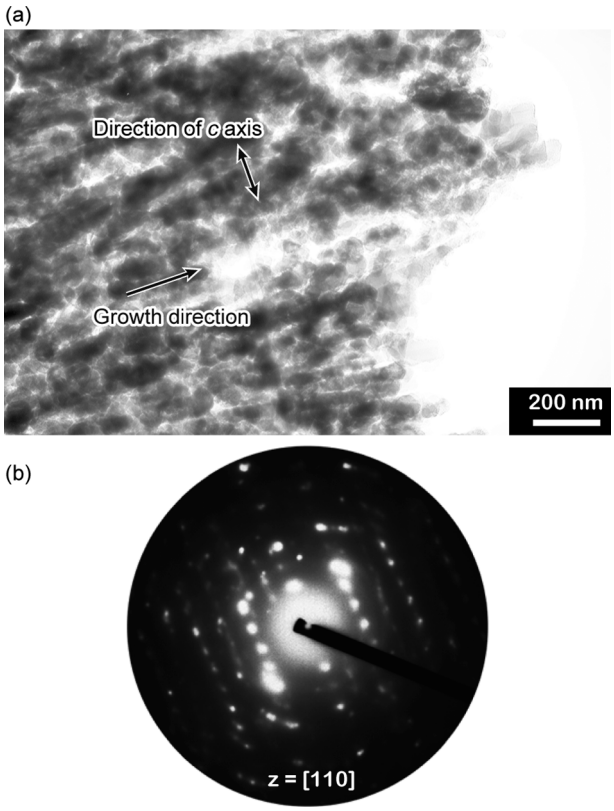

Fig. 9 (a) Bright-field TEM image and (b) corresponding SAED pattern of an isolated vaterite film grown on PNIPAm brush matrices in the presence of PAA at 40 °C.

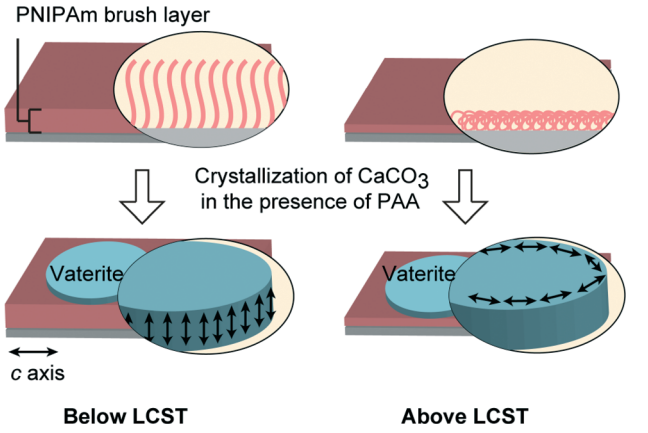

Fig. 10 Schematic illustration of vaterite thin film formation on PNIPAm brush matrices at temperatures below (20 °C) and above (40 °C) the LCST in the presence of PAA additives. Left: vaterite thin films with the *c* axis perpendicular to the substrate; right: vaterite thin films with the *c* axis parallel to the substrate.

minerals, the existence of polymer matrices may significantly influence the morphologies and polymorphs of crystals. For instance, our previous studies showed that PVA matrices preferentially induced the formation of aragonite thin films in the presence of PAA.[29,57,58] Calcite crystal thin films were obtained using chitosan,[59] chitin[28,60] and cellulose[28] matrices in the presence of PAA additives. In addition, Volkmer *et al.* reported that the use of poly(methacrylic acid) brush matrices induced the formation of amorphous calcium carbonate.[38]

We have found that the use of PNIPAm brush matrices led to the formation of vaterite thin films with distinct differences in the orientational behavior above and below the LCST (Fig. 10). For nonthermal switching systems, biomimetic vaterite thin films with preferential orientation have been reported previously by our group.[54,61] For instance, vaterite thin films with the *c* axis oriented perpendicular and parallel to the substrate in an alternating manner were formed by the cooperative effect of the chitosan matrix and the poly(aspartate) additive.[54] We have also recently reported that the synergistic effect of carboxylated polyrotaxane additives and poly(vinyl alcohol) matrices led to the formation of vaterite thin films with the *c* axis parallel to the substrate.[61] In comparison with those systems, the use of stimuli-responsive PNIPAm brush matrices enabled the possibility of tuning the crystal orientation by external stimuli.

Although the vaterite thin films formed on PNIPAm brush matrices at temperatures above and below the LCST both favoured the [1 $\bar{1}$ 0] growth direction, they have distinct preferential orientations. For thin films developed at a temperature below the LCST, the (001) plane is parallel to the film surface (Fig. 6). However, for vaterite thin films developed at a temperature above the LCST, the (110) plane is parallel to the thin film surface (Fig. 9). It is assumed that the orientational difference is attributable to the conformational change of PNIPAm chains. In addition, acidic additives such as PAA, which interact with cationic ions, are essential for the biomimetic development of hybrid thin films. The interaction between PAA and PNIPAm has also been reported.[62,63] Recent studies have also shown that acidic polymer additives induce the formation of the amorphous calcium carbonate (ACC) precursor or the polymer-induced liquid precursor (PILP).[22] The induced precursors are ionic and have fluidic character, which allow them to penetrate into PNIPAm brush matrices, resulting in the formation of vaterite thin films.

Spin-coated PNIPAm matrices cross-linked by glycerol were also employed for the crystallization of $CaCO_3$ to further examine the effect of brush structures on $CaCO_3$ crystallization (Fig. 11). For crystal thin films formed on the spin-coated PNIPAm matrices at temperatures above and below the LCST, only aragonite and calcite polymorphs are observed (Fig. 11c). To prepare a spin-coated PNIPAm matrix, a cross-linking agent is necessary to anchor the water-soluble PNIPAm. In contrast, thin films formed on PNIPAm brush matrices at temperatures above and below the LCST have vaterite polymorphs and show obvious differences in the crystallographic orientation. For the spin-coated gel and the corresponding polymer brush matrices, the difference in the conformational structures of the chains of the polymer matrices is assumed to be influential to their swelling behavior[64] and affinity with ions in aqueous solutions, thus leading to different crystallization behaviors of $CaCO_3$.

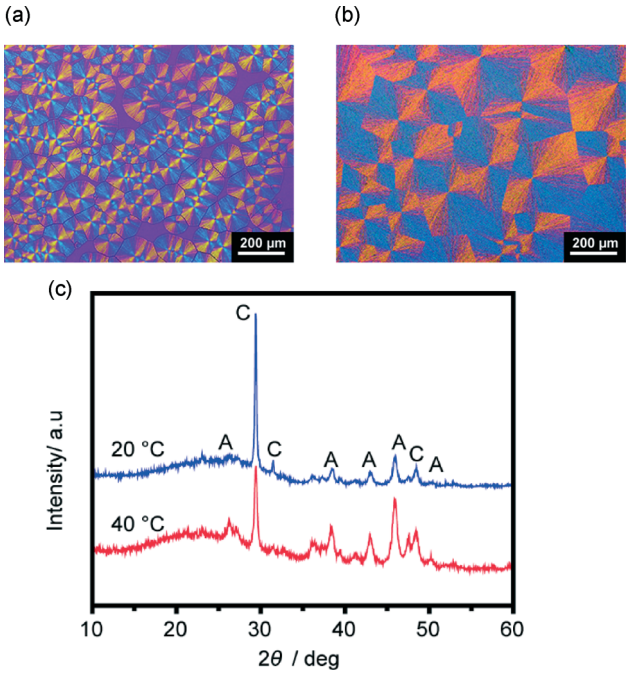

Fig. 11 Polarizing optical microscope images of $CaCO_3$ thin films formed on spin-coated PNIPAm substrates: (a) crystallization at 20 °C, (b) crystallization at 40 °C. (c) XRD patterns of corresponding thin films. A and C in XRD patterns standard for aragonite and calcite, respectively.

Conclusion

We have found that thermoresponsive PNIPAm brushes with thickness of approximately 500 nm act as effective polymer matrices for tuning the orientation and morphology of $CaCO_3$ crystal thin films. $CaCO_3$ thin films with the *c* axis preferentially perpendicular to the substrates were obtained below the LCST, while crystallization above the LCST induced the formation of vaterite thin films with the *c* axis parallel to the substrates. Oriented vaterite tablets have been found in biominerals,[56] and this study may deepen our understanding of biomineralization and could lead to a new way for developing hybrid materials.

Acknowledgements

This work was supported by a Grant-in-Aid for Scientific Research (no. 22107003) on the Innovative Areas: "Fusion Materials: Creative Development of Materials and Exploration of Their Function through Molecular Control" (area no. 2206) from the Ministry of Education, Culture, Sports, Science and Technology (MEXT).

Notes and references

1 L. Addadi and S. Weiner, *Angew. Chem., Int. Ed. Engl.*, 1992, **31**, 153.
2 E. Baeuerlein, P. Behrens and M. Epple, *Handbook of biomineralization*, Wiley-VCH, Weinheim, 2007.
3 S. Mann, *Biomineralization: principles and concepts in bioinorganic materials chemistry*, Oxford University Press, New York, 2001.
4 T. Kato, *Adv. Mater.*, 2000, **12**, 1543.
5 S. H. Yu, H. Cölfen, K. Tauer and M. Antonietti, *Nat. Mater.*, 2005, **4**, 51.
6 F. Nudelman and N. A. J. M. Sommerdijk, *Angew. Chem., Int. Ed.*, 2012, **51**, 6582.
7 T. Kato, T. Sakamoto and T. Nishimura, *MRS Bull.*, 2010, **35**, 127.
8 C. Ohtsuki, M. Kamitakahara and T. Miyazaki, *J. Tissue Eng. Regener. Med.*, 2007, **1**, 33.
9 H. B. Yao, H. Y. Fang, X. H. Wang and S. H. Yu, *Chem. Soc. Rev.*, 2011, **40**, 3764.
10 A. Sugawara-Narutaki, *Polym. J.*, 2013, **45**, 269.
11 W. L. Noorduin, A. Grinthal, L. Mahadevan and J. Aizenberg, *Science*, 2013, **340**, 832.
12 Y. Oaki, R. Adachi and H. Imai, *Polym. J.*, 2012, **44**, 612.
13 Y. Y. Kim, K. Ganesan, P. C. Yang, A. N. Kulak, S. Borukhin, S. Pechook, L. Ribeiro, R. Kroger, S. J. Eichhorn, S. P. Armes, B. Pokroy and F. C. Meldrum, *Nat. Mater.*, 2011, **10**, 890.
14 Y. Y. Kim, L. Ribeiro, F. Maillot, O. Ward, S. J. Eichhorn and F. C. Meldrum, *Adv. Mater.*, 2010, **22**, 2082.
15 Y. Oaki, S. Kajiyama, T. Nishimura, H. Imai and T. Kato, *Adv. Mater.*, 2008, **20**, 3633.
16 Y. Oaki, M. Kijima and H. Imai, *J. Am. Chem. Soc.*, 2011, **133**, 8594.
17 A. Finnemore, P. Cunha, T. Shean, S. Vignolini, S. Guldin, M. Oyen and U. Steiner, *Nat. Commun.*, 2012, **3**, 966.
18 D. K. Keum, K. M. Kim, K. Naka and Y. Chujo, *J. Mater. Chem.*, 2002, **12**, 2449.
19 Y. Tanaka and K. Naka, *Polym. J.*, 2012, **44**, 586.
20 A. Berman, L. Addadi and S. Weiner, *Nature*, 1988, **331**, 546.
21 M. Suzuki, K. Saruwatari, T. Kogure, Y. Yamamoto, T. Nishimura, T. Kato and H. Nagasawa, *Science*, 2009, **325**, 1388.
22 L. B. Gower, *Chem. Rev.*, 2008, **108**, 4551.
23 S. Kumar, T. Ito, Y. Yanagihara, Y. Oaki, T. Nishimura and T. Kato, *CrystEngComm*, 2010, **12**, 2021.
24 A. Sugawara, T. Ishii and T. Kato, *Angew. Chem., Int. Ed.*, 2003, **42**, 5299.
25 T. Sakamoto, Y. Nishimura, T. Nishimura and T. Kato, *Angew. Chem., Int. Ed.*, 2011, **50**, 5856.
26 N. A. J. M. Sommerdijk and G. de With, *Chem. Rev.*, 2008, **108**, 4499.
27 T. Kato, A. Sugawara and N. Hosoda, *Adv. Mater.*, 2002, **14**, 869.
28 N. Hosoda and T. Kato, *Chem. Mater.*, 2001, **13**, 688.
29 T. Sakamoto, A. Oichi, Y. Oaki, T. Nishimura, A. Sugawara and T. Kato, *Cryst. Growth Des.*, 2009, **9**, 622.
30 R. C. Advincula, *Polymer brushes: synthesis, characterization, applications*, Wiley-VCH, Weinheim, 2004.
31 R. Barbey, L. Lavanant, D. Paripovic, N. Schuwer, C. Sugnaux, S. Tugulu and H. A. Klok, *Chem. Rev.*, 2009, **109**, 5437.
32 A. Nomura, K. Okayasu, K. Ohno, T. Fukuda and Y. Tsujii, *Macromolecules*, 2011, **44**, 5013.
33 K. Matyjaszewski and J. H. Xia, *Chem. Rev.*, 2001, **101**, 2921.
34 J. Pyun and K. Matyjaszewski, *Chem. Mater.*, 2001, **13**, 3436.
35 M. Kobayashi and A. Takahara, *Chem. Rec.*, 2010, **10**, 208.

36 C. R. Vestal and Z. J. Zhang, *J. Am. Chem. Soc.*, 2002, **124**, 14312.
37 A. Carlmark and E. Malmstrom, *J. Am. Chem. Soc.*, 2002, **124**, 900.
38 S. Tugulu, M. Harms, M. Fricke, D. Volkmer and H. A. Klok, *Angew. Chem., Int. Ed.*, 2006, **45**, 7458.
39 A. M. Belcher, X. H. Wu, R. J. Christensen, P. K. Hansma, G. D. Stucky and D. E. Morse, *Nature*, 1996, **381**, 56.
40 M. A. Meyers, J. McKittrick and P. Y. Chen, *Science*, 2013, **339**, 773.
41 M. A. C. Stuart, W. T. S. Huck, J. Genzer, M. Muller, C. Ober, M. Stamm, G. B. Sukhorukov, I. Szleifer, V. V. Tsukruk, M. Urban, F. Winnik, S. Zauscher, I. Luzinov and S. Minko, *Nat. Mater.*, 2010, **9**, 101.
42 T. P. Russell, *Science*, 2002, **297**, 964.
43 T. Chen, R. Ferris, J. M. Zhang, R. Ducker and S. Zauscher, *Prog. Polym. Sci.*, 2010, **35**, 94.
44 H. G. Schild, *Prog. Polym. Sci.*, 1992, **17**, 163.
45 T. Sun, G. Wang, L. Feng, B. Liu, Y. Ma, L. Jiang and D. Zhu, *Angew. Chem., Int. Ed.*, 2004, **43**, 357.
46 M. Kaholek, W. K. Lee, S. J. Ahn, H. W. Ma, K. C. Caster, B. LaMattina and S. Zauscher, *Chem. Mater.*, 2004, **16**, 3688.
47 C. Y. Xue, B. C. Choi, S. Choi, P. V. Braun and D. E. Leckband, *Adv. Funct. Mater.*, 2012, **22**, 2394.
48 Y. Hou, A. R. Matthews, A. M. Smitherman, A. S. Bulick, M. S. Hahn, H. Hou, A. Han and M. A. Grunlan, *Biomaterials*, 2008, **29**, 3175.
49 Y. Kumashiro, M. Yamato and T. Okano, *Ann. Biomed. Eng.*, 2010, **38**, 1977.
50 P. M. Dove, J. De Yoreo and S. Weiner, *Biomineralization*, Mineralogical Society of America, Washington, DC, 2003.
51 H. Cölfen and S. Mann, *Angew. Chem., Int. Ed.*, 2003, **42**, 2350.
52 H. Suzuki, H. M. Nurul, T. Seki, T. Kawamoto, H. Haga, K. Kawabata and Y. Takeoka, *Macromolecules*, 2010, **43**, 9945.
53 U. Wehrmeister, A. L. Soldati, D. E. Jacob, T. Hager and W. Hofmeister, *J. Raman Spectrosc.*, 2010, **41**, 193.
54 A. Sugawara, A. Oichi, H. Suzuki, Y. Shigesato, T. Kogure and T. Kato, *J. Polym. Sci., Part A: Polym. Chem.*, 2006, **44**, 5153.
55 L. Kabalah-Amitai, B. Mayzel, Y. Kauffmann, A. N. Fitch, L. Bloch, P. U. P. A. Gilbert and B. Pokroy, *Science*, 2013, **340**, 454.
56 L. Qiao, Q. L. Feng and Z. Li, *Cryst. Growth Des.*, 2007, **7**, 275.
57 T. Sakamoto, A. Oichi, T. Nishimura, A. Sugawara and T. Kato, *Polym. J.*, 2009, **41**, 522.
58 N. Hosoda, A. Sugawara and T. Kato, *Macromolecules*, 2003, **36**, 6449.
59 T. Kato, T. Suzuki, T. Amamiya, T. Irie and N. Komiyama, *Supramol. Sci.*, 1998, **5**, 411.
60 T. Kato, T. Suzuki and T. Irie, *Chem. Lett.*, 2000, 186.
61 F. Zhu, T. Nishimura, H. Eimura and T. Kato, *CrystEngComm*, 2014, **16**, 1496.
62 M. Koussathana, P. Lianos and G. Staikos, *Macromolecules*, 1997, **30**, 7798.
63 G. Staikos, G. Bokias and K. Karayanni, *Polym. Int.*, 1996, **41**, 345.
64 A. Karim, J. F. Douglas, F. Horkay, L. J. Fetters and S. K. Satija, *Phys. B*, 1996, **221**, 331.